



Institut de Physique Nucléaire d'Orsay

Activités Scientifiques

du

Groupe de Radiochimie

# Contents

- 
- ✓ Uranyl sorption mechanisms onto titanium dioxide: from crystal to powder.....3
    - H. Perron, J. Vandenborre, R. Drot, J. Roques, E. Simoni
  
  - ✓ Simultaneous determination of uranium carbide dissolution products by capillary electrophoresis.....5
    - V. Sladkov, B. Fourest
  
  - ✓ Electrochemical behavior of uranium monocarbide in aqueous solution.....7
    - Maslennikov, B. Fourest, N. Boudanova, V. Sladkov
  
  - ✓ Irradiation effects on Thorium Phosphate Diphosphate ( $\beta$ -TPD) ; consequences on its dissolution.....9
    - C. Tamain, N. Dacheux, A. Özgümüs
  
  - ✓ Immobilization of actinides in phosphate ceramics.....11
    - N. Clavier, O. Terra, E. du Fou de Kerdaniel, N. Dacheux
  
  - ✓ Sulphate complexation of protactinium(V): Thermodynamics at tracer scale and structural characterization.....13
    - M. V. Di Giandomenico, C. Le Naour, D. Trubert
  
  - ✓ Physicochemical properties of U(IV) chloro complexes in room temperature ionic liquids.....15
    - C. Cannes, C. Le Naour, D. Trubert, S. Nikitenko
-

# Uranyl sorption mechanisms onto titanium dioxide: from crystal to powder

**IPNO Participation:** H. Perron, J. Vandendorre, R. Drot, J. Roques, E. Simoni

**Collaborations :** Laboratoire de physico-chimie et microbiologie pour l'environnement (Nancy), Laboratoire interactions et dynamique des environnements de surface (Orsay), EDF-R&D, Département Matériaux et Mécanique des Composants (Moret-sur-Loing)

## *Mécanismes d'interaction de l'uranyle avec l'oxyde de titane : du monocristal à la poudre*

*La rétention des radionucléides et leur répartition parmi différentes phases minérales co-existantes est au cœur de la gestion des déchets nucléaires. Ces dernières années, plusieurs études se sont focalisées sur la détermination de constantes de sorption fiables, en couplant une approche macroscopique et une approche microscopique. Le travail présenté ici concerne les mécanismes de sorption de l'uranyle sur une surface d'oxyde : l'oxyde de titane, phase rutile, considéré sous forme de poudre et de monocristaux. Le but est de déterminer les sites de surface actifs vis-à-vis de la sorption de l'uranyle. Dans le cas du monocristal, les plans cristallographiques sont parfaitement définis et la distribution des atomes de surface est connue. Ainsi, en comparant la sorption de l'ion uranyle selon différentes orientations cristallographiques et la sorption de ce même ion sur la poudre correspondante, les sites responsables de la rétention de U(VI) par la poudre peuvent être identifiés. De plus, ces résultats expérimentaux sont comparés à des calculs ab initio de chimie quantique.*

Within the framework of nuclear waste storage in geological repository, the safety assessment requires a complete knowledge of the mechanisms involved at the aqueous solution/mineral interface. Since radionuclides migration through the geosphere is mainly governed by sorption and precipitation phenomena, it appears to be fundamental to investigate the retention processes at a molecular level. In such a way, the major experimental limitation arises from the difficulty to extract a local phenomenon contribution from the macroscopic system. Therefore, the use of atomic scale modelling makes possible to evaluate the contribution of each component of the global system.

We present here the studies of the interaction mechanisms between uranyl ions and the rutile  $\text{TiO}_2$  oxide. This solid substrate is interesting because it can be found under both powder and single crystal forms, which allows to study the retention processes on perfectly characterized crystallographic planes. Since the repartition of the different crystallographic orientations are known for the powder, the results obtained for the single crystals can directly be used to account for the powder retention properties. By using complementary spectroscopic techniques such as Time Resolved Laser-induced Fluorescence Spectroscopy (TRLFS), X-ray Photoelectron Spectroscopy (XPS), Diffuse Reflectance Infra-red Fourier Transformed spectroscopy (DRIFT) and Surface Second Harmonic Generation spectroscopy (SSHG), it is possible to accurately determine the nature of the reactive surface sites as well as the surface species.

Furthermore, in order to better understand the interfacial interactions, atomic calculations will provide support to the experimental data by bringing complementary insights. Among all kinds of simulations, *ab initio* type calculations

are the most accurate ones, even if they can treat only small systems (from a few tens up to about one or two hundred atoms). The purpose of this part is to provide a theoretical support to the experimental investigation.

Moreover, two approaches exist to mimic the system: a periodic approach where the system is infinitely repeated in the three dimensions, and a cluster one where the system is isolated in vacuum.

## **Experimental investigation**

In a first step, the acidity properties of the solid have been investigated. The DRIFT and XPS experiments have clearly shown that the solid, in suspension in solution, is fully hydroxylated. The intrinsic acidity constants associated to the acid-base behaviour of the solid surface have been determined from the surface oxygen charges calculated using the Pauling valence bond (CD-MUSIC approach). Then, for the powdered samples, potentiometric titration experiments were performed and were successfully modelled (Constant Capacitance Model) taking into account the natural repartition of the different crystallographic planes of titania: for the studied rutile powder, the preferential crystallographic orientations are (110), (100) and (101) in the ratio 60/20/20. Thus, only the double layer inner-capacitance value remained as an adjustable parameter.

In a second step, Atomic Force Microscopy was carried out in order to verify that no surface precipitation occurs for the higher surface coverages. Moreover, these analysis have also evidenced that the U(VI) sorption is homogeneous indicating that there is no uranium cluster formation during the sorption process. These observations were corroborated by SSHG experiments (mainly for (001)), which have also

shown that the sorption occurs, in a first step, onto preferential surface symmetry axis. The spectroscopic measurements (TRLFS and XPS) clearly evidenced that there are two different surface reactive sites towards uranyl ions on both (110) and (001) crystallographic planes as well as on the powdered samples.

These sites are made up with surface oxygens linked with one or two titanium atoms, respectively. The corresponding two uranyl surface species were observed whatever the pH value ranged from 1 to 5. Nevertheless, the relative quantities of these species depend on the surface coverage (figure 1).

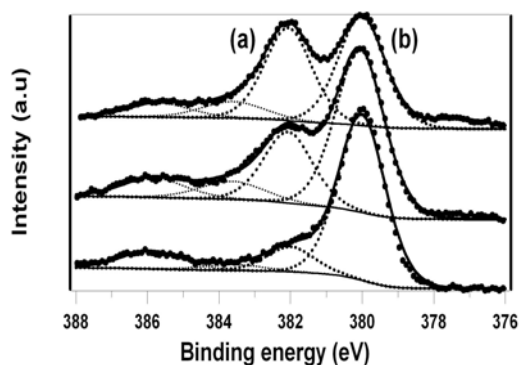


Fig. 1 :  $U4f_{7/2}$  XPS spectra of  $U(VI)$  sorbed onto (110) crystallographic face. (a) and (b) denote the two surface species.

All the spectroscopic characteristics of these uranium species (fluorescence spectra and associated decay times, binding energies) were found to be the same for the powder and (110) and (001) crystallographic planes. Moreover, DRIFT experiments have clearly shown that reactive surface oxygen atoms remained protonated after uranyl sorption indicating that all these surface atoms are not affected by the metal sorption.

Finally, the sorption edges defined for powders were then fitted on the basis of the constraints brought by the spectroscopic investigation (figure 2), which allowed to perform the fit with a minimal number of adjustable parameters and then allowed a more accurate determination of the sorption constants values.

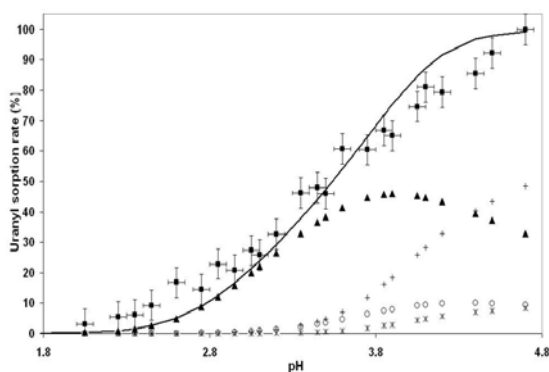


Fig. 2:  $U(VI)$ /rutile sorption edge and corresponding modelling (CCM model) according to the structural investigation

### Theoretical calculations

In the theoretical part, two different approaches, using density functional calculations, were used. First,  $TiO_2$  (110) surface was modelled with periodic slabs in order to investigate clean surface relaxations, water adsorption, and finally, interaction of uranyl ions with the mineral surface. The aim of this first step was to identify the most probable  $UO_2^{2+}$  sorption sites and to establish their relative energy stabilities as a function of the surface coverage.

Bulk rutile  $TiO_2$  as well as the (110) face parameters were optimized and were found to be in good agreement with experimental data and previous theoretical works. A five layers model, with its most internal layer frozen to bulk positions, was found to be a good model to mimic the  $TiO_2(110)$  surface. As reference data for the sorption process, hydration of the uranyl ion using periodic approach was studied. As already experimentally found, solvation energies tend to favour the pentahydrated system  $[UO_2(H_2O)_5]^{2+}$  in aqueous solution. From localized calculations, an overall 0.91 electron transfer between the first coordination shell and the uranyl ion was calculated which clearly demonstrates the importance of the solvent effect in the modelling. Then, the simulation of the uranyl ion sorption on a five layers hydroxylated  $TiO_2(110)$  model was investigated. Three different sorption sites were investigated. The saturation of the uranyl ion first coordination shell, by three water molecules, was taken into account in order to get more reliable structural parameters relative to experimental data.

Moreover, starting from the previous  $TiO_2$  (110) relaxed structure, stoichiometric  $(TiO_2)_n$  clusters were used to simulate the (110) rutile surface (figure 3). This cluster approach was done in order to study, from a local point of view, the interaction of one uranyl ion with the  $TiO_2$  (110) surface for the different possible sorption sites.

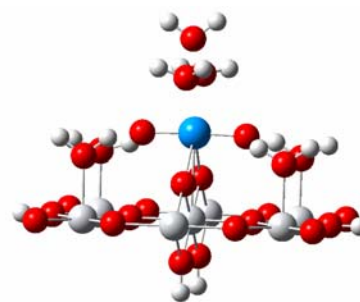


Fig. 3: Example of one cluster model used to investigate the uranyl sorption on the  $TiO_2$  (110) face.

Each theoretical result is directly compared with the experimental data summarized above and both methodologies (periodic or localized) gave similar results in agreement with these data. This original theoretical study correlated to the experimental investigation leads to an acute representation of the retention processes of radionuclides on mineral surfaces.

# Simultaneous determination of uranium carbide dissolution products by capillary electrophoresis

**IPNO Participation: V. Sladkov, B. Fourest**

## *Dosage simultané des produits issus de la dissolution du carbure d'uranium par électrophorèse capillaire.*

*La dissolution des carbures est une étape importante dans le processus de retraitement du combustible usé car il conditionne la forme des espèces solubles à séparer de manière quantitative pour la re-fabrication du combustible frais. Il apparaît donc nécessaire de connaître non seulement la quantité de carbone et d'uranium dissous dans les solutions de dissolution, mais également sous quelles formes chimiques ces éléments sont présents. Dans ce but, on a étudié les possibilités de l'électrophorèse capillaire pour le dosage simultané de U(VI) et des anions de divers acides organiques (acides mellitique, trimellitique, benzoïque et oxalique) susceptibles d'être produits lors de la dissolution des carbures.*

The electrochemical dissolution of carbide fuels in aqueous solutions leads to the formation of a number of organic species [1-2] which can cause serious interferences in the subsequent steps of reprocessing, in particular, the emulsion formation in the solvent extraction steps of the PUREX process and complexation with U(VI) resulting in an incomplete extraction of this ion [3]. The quantity of formed organic products depends on the way of dissolution (nature and concentration of electrolyte, pH, applied potential, ...). For the choice of the optimal conditions of dissolution with formation of a minimum of dissolved organic species and for uranium dissolution control, a reliable method for the simultaneous determination of organic species and U(VI) is needed.

For this application, capillary electrophoresis (CE) method was used due to the possibility of highly efficient and fast separation of species. This method has been already applied for the determination of some carboxylic anions species with direct UV detection [4-5]. The aim of the present work was to study the possibility of an adaptation of CE for a simultaneous determination of these organic anions and U(VI).

### Method

The capillary electrophoresis apparatus was a modular system consisting of a Spectrophoresis 100 injector coupled with a high voltage (0-30 kV) power supply and a scanning UV-visible detector (Prime Vision IV from Europhor). A silica capillary (75  $\mu\text{m}$  of internal diameter and around 75 cm length) was conditioned prior to its use by successive washes with deionized water and buffer solution. A hydrodynamic injection of 0.5 sec., corresponding to a volume of only one nanoliter, was used to introduce the sample into the capillary. In order to limit the uncertainties arising from temperature fluctuations, the applied voltage was limited to 15 kV. The current was thus kept below a value of 100  $\mu\text{A}$ .

Absorption spectra were recorded on a double beam spectrophotometer VARIAN (Model DMS 300) in the range 200-300 nm. The cell length was 1 cm.

Carbonate buffer solution (0.1 M) was used as the supporting electrolyte.

### Optimization of conditions

#### Spectrophotometric study

In order to optimize the detection wavelength, the absorption spectra of U(VI) and carboxylic acid species were first registered (Figure 1) in 0.1 M carbonate buffer solution at pH 9.8.

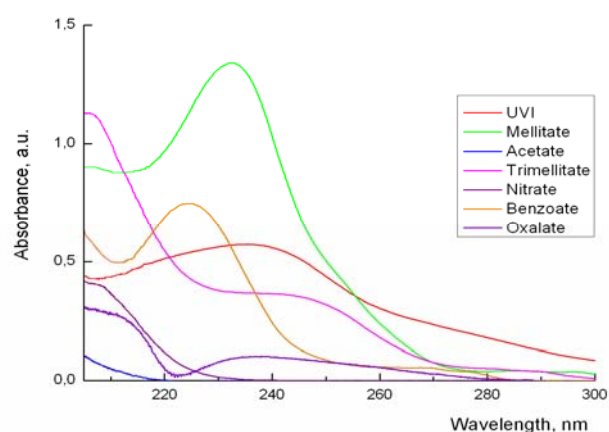


Fig. 1. Absorption spectra of  $1 \times 10^{-4}$  M U(VI),  $5 \times 10^{-5}$  M mellitate,  $1 \times 10^{-3}$  M acetate,  $5 \times 10^{-5}$  M trimellitate,  $5 \times 10^{-5}$  M nitrate,  $1 \times 10^{-4}$  M benzoate,  $5 \times 10^{-4}$  M oxalate in carbonate buffer solution (pH 9.8, 0.1 M).

From these spectra, we can observe that the absorption maxima are in the range 230-240 nm for U(VI), mellitate, and benzoate ions, and above 210 nm for trimellitate, oxalate, acetate and nitrate ions.

Two detection wavelengths, 210 nm and at 230 nm, were thus chosen for the CE experiments.

#### Optimization of the electrolyte composition

##### Effect of flow modifier concentration

In order to lower, and even to reverse, the electroosmotic flow, a flow modifier, a quaternary amine, as an alkyl ammonium salt (TTAB, tetradecyltrimethylammonium bromide) was added to the buffer. After several experiments with  $1 \times 10^{-4}$  M U(VI), the concentration of 0.15 mM of TTAB was finally chosen as optimal. As a

matter of fact, at higher concentrations (near 0.2 -0.3 mM) a precipitation process occurs (with a risk to block up the capillary) resulting in not reproducible peaks. And at lower concentrations (0.03-0.1 mM), tailings peaks are observed due to a solute anion mobility lower than the buffer anion mobility.

#### Effect of pH

Effect of pH on the peak shapes of  $1 \times 10^{-4}$  M of U(VI) was studied in the range from 9 to 11. The pH value of 9.8 was chosen for U(VI) detection, because at this pH value, only one U(VI) species is dominant (as  $\text{UO}_2(\text{CO}_3)_3^{4-}$ ) in carbonate buffer. At higher pH values, the contribution of hydrolysed species  $\text{UO}_2(\text{OH})_3^-$  is significant, and at lower pH values, another carbonate species is expected to be present ( $(\text{UO}_2(\text{CO}_3)_2)^-$ ) [6]. So, the peaks obtained at pH values not close to 9.8 are wider and, consequently, less suitable (or not suitable) for analytical measurements.

### Simultaneous determination of U(VI) and organic acid anionic species

#### Calibration curves

The calibration curves for U(VI), mellitate, trimellitate, nitrate, benzoate and oxalate ions in 100 mM carbonate buffer were plotted at 210 nm for oxalate and 230 nm for the other anions. Linear curves were obtained for one range of concentration in the case of oxalate and benzoate and two ranges in the other cases. These calibration curves were used for the further quantitative determination of dissolution products.

#### Analyses of simulation solutions

The accuracy of the procedure based on the calibration curve determination described above was checked by determining the recovery from simulation solutions, containing different quantities of U(VI) and organic acid anions. The observed electrophoresis curves are given in Figure 2. The excellent separation of products is achieved in 7 minutes without benzoate and 13 minutes with benzoate.

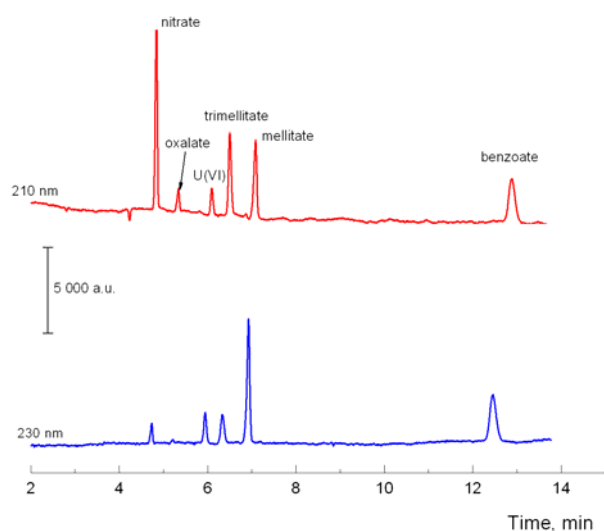


Fig. 2. Electropherograms of a simulation solution, containing of  $1 \times 10^{-3}$  M nitrate,  $8 \times 10^{-4}$  M oxalate,  $2 \times 10^{-4}$  M U(VI),  $3 \times 10^{-4}$  M trimellitate,  $5 \times 10^{-4}$  M mellitate, and  $1.5 \times 10^{-4}$  M benzoate at 210 nm and 230 nm.

The results of recovery tests are listed in Table 2. The obtained results are completely satisfying for analysis. The recovery is between 90 and 110%. The deviations from the spiked amounts are in the interval of the instrumental

Species	Amount, M		n	S <sub>r</sub> , %	Rec., %
	Added	Found			
U(VI)	$5 \times 10^{-5}$	$(4,8 \pm 0,8) \times 10^{-5}$	3	7	96
	$1 \times 10^{-4}$	$(1,0 \pm 0,1) \times 10^{-4}$	4	4,5	100
	$2 \times 10^{-4}$	$(1,9 \pm 0,1) \times 10^{-4}$	4	2	95
	$3 \times 10^{-4}$	$(3,1 \pm 0,2) \times 10^{-4}$	4	5	103
	$5 \times 10^{-4}$	$(4,9 \pm 0,1) \times 10^{-4}$	3	1	98
Oxalate	$8 \times 10^{-4}$	$(7 \pm 1) \times 10^{-4}$	3	6	88
	$1 \times 10^{-3}$	$(9 \pm 1) \times 10^{-4}$	4	11	90
	$3 \times 10^{-3}$	$(2,8 \pm 0,4) \times 10^{-3}$	4	8	93
Trimellitate	$5 \times 10^{-5}$	$(4,7 \pm 0,5) \times 10^{-5}$	3	4	94
	$7,5 \times 10^{-5}$	$(7,4 \pm 0,3) \times 10^{-5}$	4	2	99
	$1 \times 10^{-4}$	$(1,1 \pm 0,1) \times 10^{-4}$	4	3	110
	$3 \times 10^{-4}$	$(2,9 \pm 0,1) \times 10^{-4}$	4	2	97
Mellitate	$5 \times 10^{-5}$	$(5,3 \pm 0,3) \times 10^{-5}$	4	4	106
	$8 \times 10^{-5}$	$(8,1 \pm 0,3) \times 10^{-5}$	4	2	101
	$1 \times 10^{-4}$	$(1,1 \pm 0,1) \times 10^{-4}$	4	3	110
	$5 \times 10^{-4}$	$(4,6 \pm 0,2) \times 10^{-4}$	4	3	92
Benzoate	$1,5 \times 10^{-4}$	$(1,5 \pm 0,1) \times 10^{-4}$	4	3	100
	$2 \times 10^{-4}$	$(2,2 \pm 0,1) \times 10^{-4}$	3	2	110
	$5 \times 10^{-4}$	$(4,5 \pm 0,3) \times 10^{-4}$	3	3	90

method errors.

Table 1. Results of uranium(VI) and organic acid species determination in the simulation solutions. (n – number of measurements, S<sub>r</sub> – relative standard deviation, P=0.95).

### Determination of U(VI) in real uranium carbide electrochemical dissolution solutions

The same procedure was then applied for analyzing real uranium carbide electrochemical dissolution solutions. For comparison, another analytical technique (time resolved laser fluorescence spectrometry (TRLFS)) was used for the determination of U(VI). A good agreement is observed between the two methods.

### Conclusion

Capillary electrophoresis with UV-detection was adapted for the determination of uranium carbide dissolution products. The main advantage of this method is the possibility of a simultaneous determination of (almost) all the dissolution products. For some species, however, the sensitivity of UV-detection is not sufficient for their determination. A more sensitive detection mode (for example, conductivity) or a preliminary concentration is needed in these cases.

### References:

- [1] P. Pauson, J. McLean et al., Nature 197 (1963) pp. 1200
- [2] L. Ferris et M. Bradley, Journ. Am. Chem. Soc. 87 (1965) pp. 1710-1714
- [3] G. Choppin, H. Bokelund et al., Radiochim. Acta 33 (1983) pp. 229-232
- [4] C. Klampfl, et W. Buchberger, TrAC 16 (1997) pp.221-229
- [5] P. Doble et P. Haddad, J. Chrom. 834 (1999) pp. 189-212
- [6] I. Grenthe, J. Fuger et al., Chemical Thermodynamics of Uranium, NEA-OECD, North Holland (1992)

# Electrochemical behavior of uranium monocarbide in aqueous solution

**IPNO Participation: A. Maslennikov, B. Fourest, N. Boudanova, V. Sladkov**

**Collaboration : CEA-Marcoule, IPCE-RAS-Moscow**

## Comportement électrochimique du monocarbure d'uranium en solution

*L'étude de la dissolution électrochimique du monocarbure d'uranium (UC), matériau pressenti pour les Réacteurs Haute Température du futur, a été abordée sur des billes préparées par fusion à arc. Les milieux choisis pour cette étude ont été principalement  $\text{HNO}_3$  0,5 – 6,0 M et  $\text{NaOH}$  0,1 – 4,0 M, avec ou sans ajout d'ions  $\text{F}^-$  complexants. Les valeurs de potentiel de dissolution et les premières estimations de constante de vitesse et de rendement du processus ont été obtenues par application de deux méthodes : la voltammétrie cyclique et la coulométrie à sauts de potentiel. Les mécanismes de réaction aux électrodes sont ainsi apparus très différents selon le milieu choisi. La dissolution effective (vitesse de dissolution supérieure à  $50 \text{ mg cm}^{-2} \text{ h}^{-1}$ ) de UC dans  $\text{HNO}_3$  a été observée pour des potentiels de UC excédant  $1,5 \text{ V/ECS}$  avec formation de  $\text{U(VI)}$  et des efficacités de courant supérieures à 200% pour les électrolytes les plus concentrés. L'oxydation de UC dans  $\text{NaOH}$  a résulté, quant à elle, en la formation de produits peu solubles et l'efficacité de la dissolution est restée faible ( $\sim 15\%$ ) même en présence d'ions  $\text{F}^-$ .*

Uranium monocarbide (UC) or mixed carbide (U,Pu)C may find application as fuels for nuclear reactors of IVth generation. If an aqueous reprocessing of the carbide fuel is to be considered, the dissolution process of the irradiated UC (or (U,Pu)C) becomes of great importance. The recent analysis of the literature data indicates that even under strong oxidative conditions (15 M  $\text{HNO}_3$ ) UC dissolution is incomplete and complicated by the formation of a number of organic species [1-3]. The possibility to increase the yield of UC dissolution and the destruction of accumulated organic species by application of electrochemical techniques was demonstrated [4-5]. However, the development of a reliable technique for the UC dissolution requires a fundamental knowledge of the electrochemical properties of this compound. The present study was aimed to the electrochemical investigation of UC dissolution in 0.5-6.0 M  $\text{HNO}_3$ , and 0.1-4.0 M  $\text{NaOH}$ .

### Method

UC microspheres of 4 mm diameter pressed into a Teflon tip and connected to an EDI101T rotating disk electrode (RDE) assembly (Radiometer) were used as the working electrode in a three-electrode system comprising also a  $\text{Hg/Hg}_2\text{Cl}_2$  reference electrode and a Pt wire counter electrode. Cyclic voltammetry (CV) and multistep potential sweep coulometry (MPSC) were applied to determine the main UC electrochemical characteristics.

### CV Results

As shown in Fig. 1 and 2, CV curves indicate three ranges of potentials, corresponding to different processes occurring at the UC electrode.

In the range from 0 to 400 mV, the UC electrode is found in a passive state, corresponding to the formation of an uranium oxycarbide ( $\text{UC}_{1-x}\text{O}_x$ ) protective layer on the oxidized surface.

At potentials exceeding 400 mV, a rapid increase of the anodic current density is observed which leads to a peak value at 1100-1400 mV in 0.1-4.0 M  $\text{NaOH}$  and to a plateau between 500 and 1300 mV in 0.5-4.0  $\text{HNO}_3$ . In the former medium, the current density increase can be associated either with the UC dissolution (accompanied with  $\text{CO}_2$  formation) or with an  $\text{O}_2$  evolution. In the latter one, it corresponds to a pseudopassivation phenomenon of the UC electrode resulting from two simultaneous reactions:  $\text{UC}_{1-x}\text{O}_x$  accumulation at the electrode surface and its further oxidation with formation of soluble products.

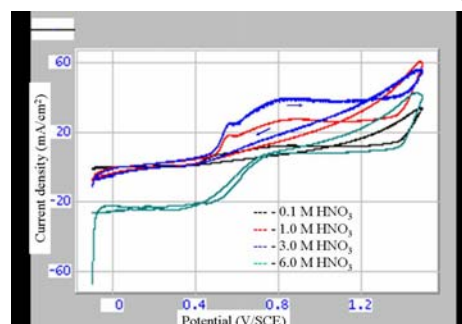


Fig. 1 : CV curves at UC electrode in 0.1-6.0 M  $\text{HNO}_3$ ,  $dE/dt=10 \text{ mV s}^{-1}$ ,  $t=25^\circ\text{C}$ .

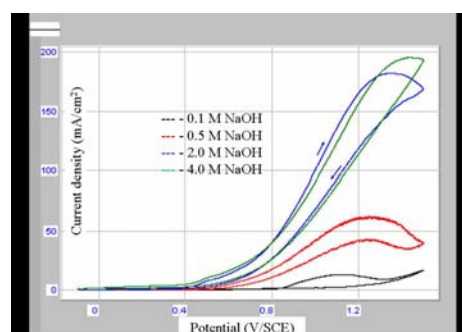


Fig. 2 : CV curves at UC electrode in 0.1-4.0 M  $\text{NaOH}$ ,  $dE/dt=10 \text{ mV s}^{-1}$ ,  $t=25^\circ\text{C}$ .

*Arrows show the direction of the potential scan.*

The increase of the plateau current density with the increase of HNO<sub>3</sub> concentration is proportional to the ratio of the rate constants of the mentioned reactions. At potential values higher than 1300 mV, an intensive UC dissolution is observed. The change of the potential scan direction at 1500 mV results in a current density hysteresis, which may be accounted for the increase of the electrode-electrolyte interface due to a pitting dissolution mechanism.

The peculiar electrochemical UC behavior in HNO<sub>3</sub> solutions with concentrations more than 4.0 M is associated with the NO<sub>3</sub><sup>-</sup> ions and HNO<sub>2</sub> reduction occurring at potential values less than 700 mV. However, the increase of HNO<sub>3</sub> concentration to 6.0 M does not shift the potential of UC dissolution to more positive values.

The addition of F<sup>-</sup> ions able to form stable complexes with the products of UC oxidation, U(IV) and U(VI), results in an increase of the UC dissolution rate only in HNO<sub>3</sub> solutions and in the narrow range of potentials from 800 to 1100 mV. The further increase of potential results in a current decrease, proving the secondary passivation of the UC electrode.

From CV data, UC electrochemical dissolution rates were estimated by assuming that U(VI) and CO<sub>2</sub> are the final products of UC oxidation in aqueous solutions. The so-calculated kinetics data are 55-75 mg·cm<sup>-2</sup>·h<sup>-1</sup> in 2.0-4.0 M HNO<sub>3</sub> and 140-190 mg·cm<sup>-2</sup>·h<sup>-1</sup> in 2.0-4.0 M NaOH.

## MPSC results

MPSC measurements included the registration of I-t curves, at a constant potential, E, during 1 min, in the range from the open circuit potential E<sub>T=0</sub> to 1500 mV, by step of 50 mV. Each I-t curve was integrated in order to obtain the charge (Q, mC) passed through the cell. The analysis of MPSC data shows that, in the range of potentials corresponding to the UC anodic dissolution, I-t curves in both HNO<sub>3</sub> and NaOH were characterized by a minimum, observed at t=5-10 s, followed by an increase of the current density to a constant value. The observed current density drop may be associated with the immediate increase of the surface film resistance after application of the anodic potential pulse, followed by its dissolution with a rate proportional to the applied potential.

From the integrated charge values, the uranium concentrations, supposed to be oxidized into U(VI) in the resulting electrolyte, were calculated. These data can be compared in Table 1 to the U(VI) concentrations, determined using the laser-induced fluorescence technique (LIF). The current efficiency, CE, values in HNO<sub>3</sub> solutions are greater than 100% in all the studied range of acid concentration and exceeds 200% in 4.0-6.0 M HNO<sub>3</sub>. This overestimation may be accounted for an increasing role of the chemical oxidation in HNO<sub>3</sub> solutions with concentration exceeding 4.0 M. The CE values for the UC electrochemical dissolution in NaOH never exceed 16%, indicating the formation of low-soluble UC oxidation products, apparently mono- or polyuranates. Therefore, the

significant current densities observed at UC electrode in NaOH solutions at the potentials between 800 and 1500 mV are associated with the water decomposition at the electrode surface rather than UC anodic dissolution.

Electrolyte	[U(VI)], M Q-E measurements	[U(VI)], M LIF technique	CE, %
0.5 M HNO <sub>3</sub>	(1.10±0.05)·10 <sup>-4</sup>	(1.70±0.09)·10 <sup>-4</sup>	162.3
1.0 M HNO <sub>3</sub>	(1.35±0.07)·10 <sup>-4</sup>	(2.12±0.11)·10 <sup>-4</sup>	153.2
2.0 M HNO <sub>3</sub>	(1.78±0.09)·10 <sup>-4</sup>	(1.92±0.09)·10 <sup>-4</sup>	107.3
3.0 M HNO <sub>3</sub>	(1.54±0.06)·10 <sup>-4</sup>	(1.54±0.05)·10 <sup>-4</sup>	122.9
4.0 M HNO <sub>3</sub>	(9.05±0.05)·10 <sup>-5</sup>	(2.02±0.10)·10 <sup>-5</sup>	217.7
6.0 M HNO <sub>3</sub>	(7.55±0.05)·10 <sup>-5</sup>	(2.10±0.12)·10 <sup>-5</sup>	277.3
0.5M NaOH	(1.57±0.04)·10 <sup>-4</sup>	(1.32±0.04)·10 <sup>-5</sup>	8.5
1.0M NaOH	(3.05±0.06)·10 <sup>-4</sup>	(1.42±0.04)·10 <sup>-5</sup>	4.7
2.0M NaOH	(4.24±0.06)·10 <sup>-4</sup>	(6.56±0.05)·10 <sup>-5</sup>	15.5
4.0M NaOH	(7.03±0.08)·10 <sup>-4</sup>	(3.74±0.04)·10 <sup>-5</sup>	5.3

Table 1: Comparison of U(VI) concentrations calculated from Q-E measurements and determined using laser fluorescence technique.

## Conclusion

This investigation of UC electrochemical dissolution showed that the mechanism of the electrode reactions depends strongly on the electrolyte chosen for the dissolution. In HNO<sub>3</sub> the dissolution is effective (dissolution rates higher than 50 mg·cm<sup>-2</sup>·h<sup>-1</sup>) at potentials exceeding 1300 mV, with formation of U(VI). The contribution of UC chemical oxidation is also important in 4.0-6.0 M HNO<sub>3</sub> providing a current efficiency more than 200%. The oxidation of UC in NaOH results in the formation of low-soluble products and the efficiency of the dissolution (about 15%) is not improved by the introduction of complex forming agent (F<sup>-</sup>) into the electrolyte. The suppositions about the mechanism of UC electrochemical dissolution require experimental proofs using techniques allowing the calculations of the process material balance, for example, potential controlled electrolysis. This study is now being under progress.

## References:

- [1] C. Terrassier, *Etude de la formation d'acides organiques à partir de carbone à l'état de traces en milieu acide et oxydant*. Ph.D. Thesis, Université Paris VI, France (March 2003).
- [2] G. R. Choppin, H. Bokelund, M. S. Caceci, S. Valkiers. *Radiochim. Acta* 34 (1983) 151.
- [3] V. Chandramouli, N. L. Sreenivasan, R. B. Yadav, *Radiochim. Acta* 51 (1990) 23.
- [4] V. H. Von Bildstein, K. Knotik, *Kerntechnik* 8 (1966) 110.
- [5] A. Palamalai, S. K. Rajan, S.K. Rajan, Chinnusamy, M. Sampath, P.K. Varghese, T.N. Ravi, V.R. Raman, G.R. Balasubramanian. *Radiochim. Acta* 55 (1991) 29.

# Irradiation effects on Thorium Phosphate Diphosphate ( $\beta$ -TPD) ; consequences on its dissolution.

**IPNO Participation:** C. Tamain, N. Dacheux, A. Özgümüs

**Collaboration :** CSNSM, CIRIL, ITU

## Effets de l'irradiation sur le Phosphate Diphosphate de Thorium ( $\beta$ -PDT) ; conséquences sur sa dissolution

*Le Phosphate Diphosphate de Thorium (PDT), matrice candidate pour assurer l'immobilisation à long terme des actinides en site géologique profond, doit présenter une bonne résistance à l'irradiation. Des échantillons frittés de PDT ont été soumis à des irradiations sous faisceau d'ions de différentes énergies pour étudier les effets de l'irradiation sur la structure puis la tenue à l'altération aqueuse après irradiation. L'amorphisation du matériau a été suivie par diffraction sous rayons X. Elle est complète sous faisceau d'ions Kr (840 MeV). En revanche, elle n'est que partielle pour une irradiation avec des ions S (450 MeV) à  $5 \cdot 10^{13} \text{ cm}^{-2}$ . D'après des observations par MEB, l'irradiation sous faisceaux d'ions semble conduire à une réduction de la porosité globale. Des tests de lixiviation ont été réalisés sur des échantillons frittés préalablement irradiés. La phase amorphisée sous irradiation présente une cinétique de dissolution plus élevée que la phase non irradiée, différence d'autant plus grande que la fraction amorphe du matériau est importante.*

The  $\beta$ -Thorium Phosphate Diphosphate ( $\beta$ -TPD),  $\text{Th}_4(\text{PO}_4)_4\text{P}_2\text{O}_7$ , can be presented as a potential field of actinide-bearing phase for nuclear waste storage in the geological disposal. This ceramic can be loaded with a large amount of tetravalent actinides like plutonium exhibits a high resistance to aqueous corrosion and a high thermal stability. Nevertheless self-irradiation by alpha-decays due to the actinides could modify its performances. Thus, it appears necessary to study the effects of self-irradiation on the chemical and physical properties of the ceramic. Self-irradiation was mainly simulated by external exposition to radiation. Samples were irradiated then submitted to dissolution tests. Other simulations were performed by internal irradiation through the loading of samples with  $^{239}\text{Pu}$  then leaching of the samples.

## Irradiation effects on $\beta$ -TPD structure

The structural effect of irradiation was first studied using high energetic heavy ions and X-Ray Diffraction (XRD) analysis. High energetic heavy ions as  $\gamma$ -rays interact with the matrix only by ionization effect (electronic contribution to amorphization) except at the end of the path of the ion (nuclear contribution to amorphization). Critical doses of amorphization were determined. No structural effects were observed for  $\gamma$ -ray irradiations even for high doses (1 MGy). The ions have enough energy to cover several tens of micrometers, which represents a sufficient thickness for dissolution studies.

Ion beam irradiations were performed with high energy ions (840 MeV krypton, 450 MeV xenon, 410 MeV sulphur and 170 MeV iodine). It enables to determine the behaviour of  $\beta$ -TPD versus the electronic loss (figure 1). Irradiations with low energy ions (5 MeV gold) were also performed to study the influence of nuclear energy loss.

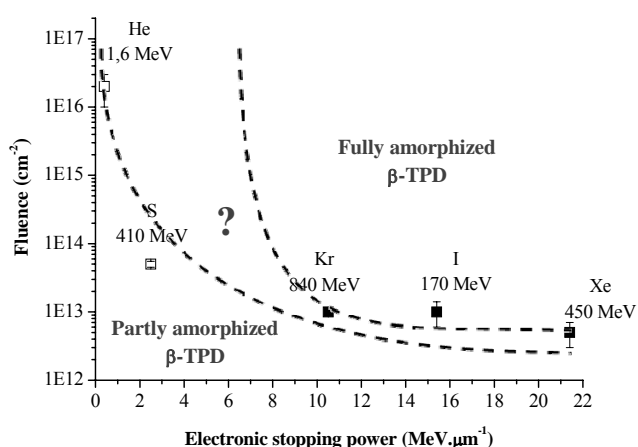


*Fig. 1: Influence of the electronic LET on the fluence on fully amorphization of  $\beta$ -TPD irradiated under energetic ion beams (■ : fully amorphization observed ; □ : partly amorphization observed)*

It appeared that the ceramic was completely amorphized with ions of energy loss higher than  $10 \text{ MeV} \cdot \mu\text{m}^{-1}$ . For energy loss lower than  $4 \text{ MeV} \cdot \mu\text{m}^{-1}$ , a threshold appears: the material does not reach an amorphous state even with high fluences. The main vibration bands observed in the  $\mu$ -Raman spectra of irradiated samples were not significantly

affected compared to the raw material. The figure 2 represents the SEM micrograph of the border between the irradiated and the non irradiated zone on a sample. It illustrates the modification of the porosity of the material under irradiation at the microscopic scale.

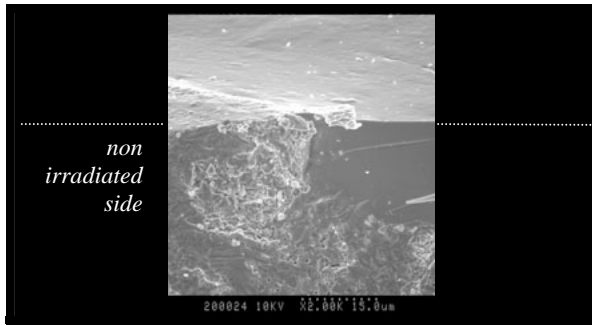


Fig 2: SEM micrograph of the border between the irradiated and the non irradiated zone on a sample.

Annealing studies were also performed: amorphous irradiated  $\beta$ -TPD can be recrystallized thanks to thermal annealing at 750°C for 10 hours. Activation energy of thermal annealing was estimated to 2.8 eV.

For Pu-loaded samples, the unit cell parameters are not modified even after several months of ageing (cf. Table 1) which reveals a good resistance of the material to internal irradiation.

Age (months)	a (Å)	b (Å)	c (Å)	V (Å <sup>3</sup> )
0	12.779(6)	10.365(3)	7.027(3)	930(1)
16	12.770(1)	10.362(7)	7.013(6)	928(2)
36	12.763(9)	10.366(7)	7.023(7)	929(2)
90	12.778(1)	10.380(1)	7.034(1)	929(2)

Table 1: Evolution of the unit cell parameters of solid solutions of  $\text{Th}_3\text{Pu}(\text{PO}_4)_4\text{P}_2\text{O}_7$ .

## Leaching tests of irradiated samples

The dissolution tests were preferentially carried out on  $\beta$ -TUPD solid solutions to allow the use of uranium as a tracer of the dissolution. Indeed, contrary to thorium which quickly precipitates with phosphate anions, U(IV) is oxidized into uranyl then remains in solution and can be determined with a good accuracy.

The dissolution of fully and partly amorphous matrices was studied considering several conditions (temperature,

acid concentration). From these results, the increase of the uranium release in  $10^{-1}\text{M}$   $\text{HNO}_3$  is about one order of magnitude from the raw material ( $7 \cdot 10^{-4} \text{ g.m}^{-2}.\text{d}^{-1}$  at 90°C) to the fully amorphized sample ( $9.9 \cdot 10^{-3} \text{ g.m}^{-2}.\text{d}^{-1}$  at 90°C) (Fig. 3).

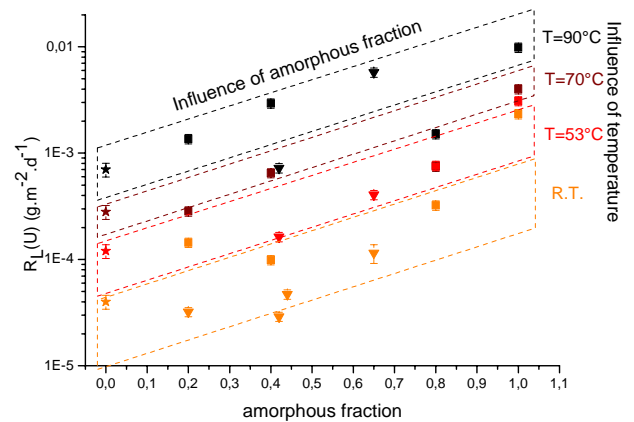


Fig 3: Influence of the amorphization on the normalized dissolution rate in  $10^{-1}\text{M}$   $\text{HNO}_3$ , at several temperatures (raw samples ( $\star$ ) or samples irradiated with Kr 840 MeV ( $\blacksquare$ ) or S 450 meV ( $\blacktriangledown$ )).

The kinetics of dissolution depends on the amorphous fraction of the  $\beta$ -TPD or  $\beta$ -TUPD. But the thermodynamics is quite similar in all the cases: the saturation of the medium leads to the precipitation of thorium under a neoformed phase identified as  $\text{Th}_2(\text{PO}_4)_2(\text{HPO}_4)\cdot\text{H}_2\text{O}$  (TPHPH). As in the case of unirradiated samples, this phase significantly delays the release of radionuclides thanks to a diffusion regime.

For complementary *in situ* experiments, the loading with  $^{239}\text{Pu}$  does not affect the resistance of the ceramics to aqueous alteration (Table 2). Actually the substitution of thorium by plutonium 239 does not significantly modify the normalized dissolution rate. Further investigations should be performed soon with  $^{238}\text{Pu}$  in order to increase the radiolytic phenomena of the dissolution of the ceramics.

$[\text{H}_3\text{O}^+]$	$\text{Th}_{3.6}\text{Pu}_{0.4}\text{P}_6\text{O}_{23}$	$\text{ThU}_3\text{P}_6\text{O}_{23}$
$10^{-1}\text{M}$	$(5.8 \pm 0.3) \cdot 10^{-6}$	$(2.5 \pm 0.2) \cdot 10^{-5}$
$10^{-2}\text{M}$	$(4.3 \pm 0.4) \cdot 10^{-6}$	not measured
$10^{-3}\text{M}$	$(3.5 \pm 0.2) \cdot 10^{-6}$	$(4.9 \pm 0.2) \cdot 10^{-6}$
$10^{-4}\text{M}$	$(2.4 \pm 0.1) \cdot 10^{-6}$	$(1.2 \pm 0.3) \cdot 10^{-6}$

Table 2: Normalized dissolution rate ( $\text{g.m}^{-2}.\text{d}^{-1}$ ) of solid solutions at 25°C in several media.

# Immobilization of actinides in phosphate ceramics

**IPNO Participation:** N. Clavier, O. Terra, E. du Fou de Kerdaniel, N. Dacheux

**Collaboration :** CEA Cadarache, LCSM (Nancy), CDGA (Bordeaux)

## *Immobilisation des actinides dans des céramiques phosphatées*

*Le Phosphate-Diphosphate de Thorium, les monazites, les brabantites et les britholites sont considérés comme des matrices potentielles d'immobilisation des actinides tri- et tétravalents en vue d'un stockage géologique en profondeur. La capacité de ces matériaux à incorporer des actinides tétravalents a été étudiée en détail en utilisant des méthodes de synthèses impliquant des procédés par voies sèches ou humides. Le frittage de ces matériaux a aussi été examiné avec attention et des échantillons denses ont été obtenus en optimisant les conditions de frittage pour chaque matériau. Les échantillons ont été caractérisés en utilisant des techniques d'analyses variées (DRX, MEB, MASE, spectroscopies infrarouge et  $\mu$ -Raman). Une étude portant sur la résistance à l'altération de ces matériaux a aussi été entreprise. Un schéma de dissolution du  $\beta$ -PDTU a été proposé et des résultats relatifs à la lixiviation des trois autres matrices ont été obtenus. Les mécanismes de dissolution des monazites, des brabantites et des britholites sont actuellement en cours d'identification.*

In order to immobilize tri- and tetravalent actinides coming from the reprocessing of nuclear waste and/or dismantled nuclear weapons in an underground repository, several storage matrices were chosen to be extensively studied, including a zirconium titanate: zirconolite ( $\text{CaZrTi}_2\text{O}_7$ ) and three phosphate matrices: monazites ( $\text{Ln}^{\text{III}}\text{PO}_4$ ) and associated brabantites ( $\text{CaAn}^{\text{IV}}(\text{PO}_4)_2$ ), britholites ( $\text{Ca}_9\text{Nd}_{1-x}\text{An}^{\text{IV}}(\text{PO}_4)_{5-x}(\text{SiO}_4)_{1+x}\text{F}_2$ ) and Thorium Phosphate-Diphosphate and its associated solid solutions ( $\beta\text{-Th}_{4-x}\text{An}_x(\text{PO}_4)_4\text{P}_2\text{O}_7$ ) as well as the field of  $\beta\text{-T(U)PD/monazite}$  composites. The incorporation of thorium and uranium into these matrices was studied in the french research group NOMADE. For each matrix, the chemical formula was optimized for the incorporation of a minimum of 10 wt.% of actinide. The Radiochemistry Group of IPNO has particularly studied the three phosphate matrices. Different chemical routes of synthesis were developed for each matrix and an optimization of the sintering of these materials was realized.

In order to study the long term behaviour of the materials, the chemical durability was examined through several leaching tests.

### Synthesis

The syntheses of such materials were developed using wet and dry chemical routes. Wet chemical routes were used to prepare monazite and  $\beta\text{-T(U)PD}$ . A precursor of these solids was first precipitated mixing the solutions of cations and concentrated phosphoric acid in the stoichiometric mole ratio of the expected compound. The mixture was then placed on a sand bath at  $150^\circ\text{C}$  or in autoclave for higher temperatures ( $160^\circ\text{C}$ - $200^\circ\text{C}$ ) during 5 to 10 hours for  $\beta\text{-T(U)PD}$  and for about 15 days for monazite samples. A crystallized precipitate which was identified as Thorium (Uranium) Phosphate-Hydrogenophosphate Hydrate ( $\text{T(U)PHPH}$ ) for the  $\beta\text{-T(U)PD}$  and monazite or rhabdophane for the monazite (depending on the average ionic radius of the cations) has been obtained. This one was separated from the solution by centrifugation. It was then washed, dried, and heated at high temperature ( $1100^\circ\text{C}$ -

$1300^\circ\text{C}$ ) in order to reach the final ceramic expected. The XRD analysis showed that all the compounds were single phase [1].

The dry chemical route was used to prepare brabantites and britholites. The actinides and the lanthanides were introduced as oxides, while the other cations were introduced as phosphate and fluoride compounds for britholites. The reactive powders underwent a manual grinding followed by a mechanical step in order to homogenize the initial powdered mixture and to improve its reactivity. A high temperature heating treatment ( $1300$ - $1400^\circ\text{C}$ ) was finally realized to obtain the expected material [2].

### Sintering and characterization

Sintering was also undertaken on these compounds. Indeed, if such materials were used to store actinides coming from nuclear waste in an underground repository, a compact shape is required. For  $\beta\text{-T(U)PD}$  as well as for monazite, the initial precursor powder was then pressed from 200 to 800 MPa in a cylindrical shape. After heating at  $1250^\circ\text{C}$  for 10 hours, dense pellets of  $\beta\text{-T(U)PD}$  were obtained with 95% to 99% of the calculated density. On the contrary, the remaining porosity was high for the monazite after 10 hours at  $1300^\circ\text{C}$ . A hot-pressing sintering was then realized to improve the density of the final pellets. The first heating treatment was realized at  $150^\circ\text{C}$  for 1 hour. The pellets were then heated at  $800^\circ\text{C}$  for 15 minutes under vacuum and then finally at  $1150^\circ\text{C}$  in inert atmosphere and under a pressure of 15-30 MPa. By this way, the relative density reached 95% to 99%. SEM micrographs (Fig. 1) show the good densification of both materials after sintering. Grain boundaries are visible on the surface of the  $\beta\text{-T(U)PD}$  pellet while no trace of the initial morphology of the grains is visible in the bulk. The hot pressed monazite shows no trace of the initial morphology of the grains at the surface and in the bulk. These observations agree well with the good densification of both materials in these sintering conditions [3].

Brabantite and britholite followed a rather different way of sintering than the previous ones. For the brabantites, the mixture of powders obtained at room temperature was heated at 800°C during 8 hours. Afterwards, a mechanical grinding was achieved (30Hz, 15min.) and the powder was shaped under a pressure of 200-800 MPa. The pellets were then heated at 1300°C for 10 hours and after heating, dense pellets with 90 to 95% of the calculated density were obtained. Likely to the brabantite, the mixture of powder mechanically ground was first heated at 1390°C for 6 hours for the britholite. Three mechanical grindings were then realized (20Hz, 10min.) and the powder was uniaxially pressed (200-800 MPa). The final heating treatment was undertaken and dense pellets were then obtained (97-98% of the relative density). For both solids, this way of sintering gave samples with very high densities [2]. Several characterizations of the samples were undertaken through EPMA, XRD,  $\mu$ -Raman and/or infrared spectroscopies. All these analyses showed single phase compounds with the expected chemical composition.

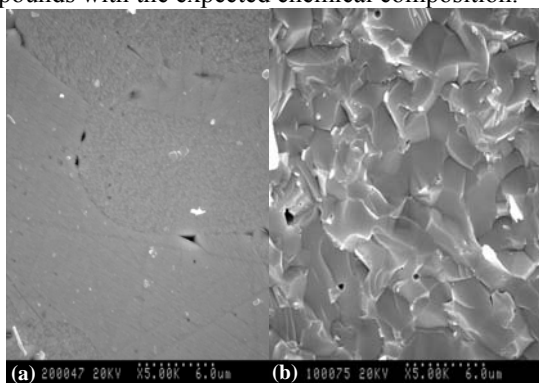


Fig 1: SEM observations of the surface of a hot pressed monazite (a) and of the bulk of uniaxially pressed  $\beta$ -TUPD (b)

### Study of the chemical durability

In order to make the evidence of the successive steps occurring during the dissolution of  $\beta$ -TUPD solid solutions, the behaviors of uranium and thorium were examined during the leaching tests. Due to its rapid oxidation in uranyl, uranium was preferentially released in the leachate. On the contrary, thorium was quickly precipitated in neoformed phosphate-based phases which acted afterwards as a protective layer inducing diffusion processes. This observation was correlated with the two different dissolution rates observed for uranium :  $2.1 \cdot 10^{-5} \text{ g m}^{-2} \text{ day}^{-1}$  during the first days of leaching then  $9.9 \cdot 10^{-6} \text{ g m}^{-2} \text{ day}^{-1}$  in the second part of the dissolution curves ( $10^{-3} \text{ M HNO}_3$ ,  $T = 50^\circ\text{C}$ ). EPMA and SEM were undertaken on leached samples. According to SEM observations and EPMA results, the bulk material seemed to be unaffected by the dissolution which occurred preferentially inside the grain boundaries at the surface of the pellets without any modification of the chemical composition of the solid leading to a non-stoichiometric dissolution.

As expected from the thorium behavior during leaching tests, neoformed phases were quickly formed at the surface of the leached pellets. The first appeared as “spiderweb” and seemed to be amorphous. The second was composed of ovoid plates of 2 to 8  $\mu\text{m}$  in length and formed bigger aggregates of 10 to 15  $\mu\text{m}$ . The mole ratios Th/P and U/(U

+ Th) determined from EPMA experiments on these phases were found to  $0.69 \pm 0.01$  and  $0.02 \pm 0.01$ , respectively, showing a significant depletion of uranium (compared to 0.36 found for the raw sample) which appeared in good agreement with the formation of pure  $\text{Th}_2(\text{PO}_4)_2\text{HPO}_4 \cdot \text{H}_2\text{O}$  (TPHPH).

In order to confirm the precipitation of TPHPH onto the surface of  $\beta$ -TUPD samples,  $\mu$ -Raman analyses were also performed. The observation of all the vibration bands associated to both P-O bonds and P-O(H) edge and the absence of those associated to the P-O-P bridge characteristic of diphosphate groups agreed well with the formation of TPHPH. Moreover, the presence of a continuous background in the 800-1200  $\text{cm}^{-1}$  region was characteristic of an amorphous phase which was certainly associated to the “spiderweb” observed by SEM. The spectra recorded on the uncovered surface revealed no difference with the unleached samples, confirming that the dissolution did not significantly modified the solid from a structural point of view [1].

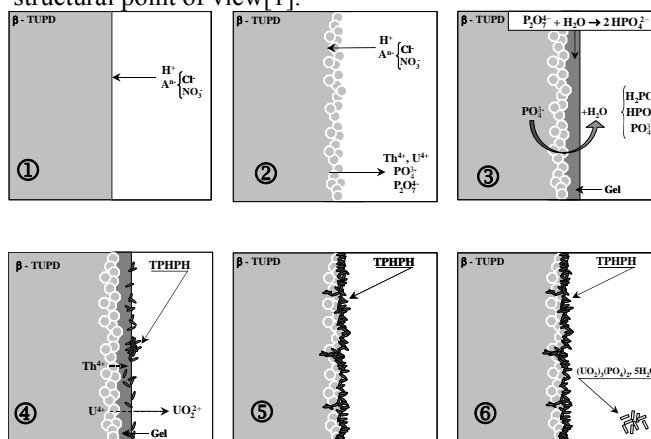


Fig 2: Proposition of a schematic mechanism of the  $\beta$ -TUPD dissolution

The dissolution of the monazite, brabantite and britholite is still under study. Some leaching rate values were obtained in acidic media for several pH and temperatures in static and dynamic conditions. For the monazite, depending on the medium acidity and the temperature, the leaching rates were between  $4 \cdot 10^{-5}$  and  $2 \cdot 10^{-3} \text{ g m}^{-2} \text{ day}^{-1}$ . For the brabantites, the results appeared nearly the same. The dissolution appeared to be congruent and the leaching rate values were found from  $6 \cdot 10^{-5}$  to  $2 \cdot 10^{-4} \text{ g m}^{-2} \text{ day}^{-1}$  depending on the pH considered. All the leaching tests for the brabantites were made at 90°C. These leaching rates values were close to that found in the literature for natural monazites. For britholites, thorium, silicon, calcium, and neodymium precipitate very quickly as neoformed phases (probably as phosphate-based phases). However, further experiments need to be undertaken in order to characterize precisely these neoformed phases and to complete the data bank associated to the normalized dissolution rates for all these materials.

### References :

- [1] N. Clavier, thèse de l'université Paris SUD, IPNO-T-04-15, 2004
- [2] O. Terra, thèse de l'université Paris SUD, IPNO-T-05-03, 2005
- [3] N. Clavier *et al.*, *Chem. Mater.*, 16, 2004, 3357-3366.

# SULPHATE COMPLEXATION OF PROTACTINIUM(V) : Thermodynamics at tracer scale and structural characterization

**IPNO Participation: M. V. Di Giandomenico, C. Le Naour, D. Trubert**

**Collaboration : CEA Valrho, ITU Karlsruhe, ESRF/ROBL Grenoble, Actinet Network**

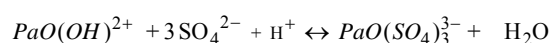
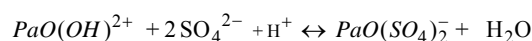
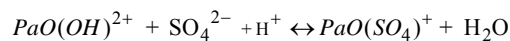
## **Complexation du protactinium(V) en milieu sulfate : approche thermodynamique et structurale**

*La complexation du protactinium(V) en milieu sulfate a été étudiée à l'échelle des traces ( $^{233}\text{Pa} \sim 10^{-12} \text{ M}$ ) et à 25°C en fonction de la force ionique du milieu dans le système  $\text{Pa(V)}/\text{H}_2\text{O}/\text{SO}_4^{2-}/\text{H}^+/\text{Na}^+/\text{ClO}_4^-$  par la technique d'extraction par solvant avec l'agent chélatant thenoyltrifluoroacétone (TTA) dans le toluène. Les constantes de complexation ont été déterminées et une modélisation de type SIT permettra d'extrapoler ces valeurs thermodynamiques à force ionique nulle ainsi que les coefficients d'interaction spécifique afférents. Pour la première fois, des déterminations structurales de complexes de  $\text{Pa(V)}$  ont été effectuées par spectroscopies SAX (XANES et EXAFS). Les résultats ont clairement indiqué la présence d'un motif mono-oxo, contrairement aux autres éléments actinides (U, Np, Pu, Am) qui présentent tous un motif trans-di-oxo.*

Information about the speciation of Pa(V) in complexing or non-complexing media are scarce in the literature and often controversial [1,2]. This discrepancy is related to the intrinsic properties of this element, characterized by a strong tendency towards hydrolysis, colloid and polymer formation. The high affinity of Pa(V) for any solid support and impurities in solution enhances experimental difficulties encountered when working with this element, leading to irreproducible results.

Sulphate is one of the mostly complexing agent used (with fluoride ions) for the study of protactinium chemistry. However, even if their complexation ability was widely used in the past for analytical and/or separation purposes, only few studies were dedicated to the identification of the species involved and only two papers were devoted to the determination of complexation constants in terms of thermodynamics.

In sulphate acidic media ( $\text{H}^+ \geq 0.1 \text{ M}$ ), depending upon sulphate concentration, the following equilibria can occur:



The aim of the present work is to determine both complexation constants of protactinium(V) in the aqueous system  $\text{Pa(V)}/\text{H}_2\text{O}/\text{SO}_4^{2-}/\text{H}^+/\text{Na}^+/\text{ClO}_4^-$  as a function of proton concentration, ionic strength and temperature and the species structure by means of XAS measurements.

### **1 Thermodynamics at tracer scale**

The main problem that arises with sulphate ions in acidic solution is the calculation of the concentrations of the free ions in the medium (particularly for high ionic strength). Therefore, a computer code was developed in order to determine from the starting constituents ( $\text{NaClO}_4$ ,  $\text{HClO}_4$  and  $\text{Na}_2\text{SO}_4$ ) the final concentrations of the free ions in solution. Coherence of calculated data

was checked by performing measurements of total and free proton concentrations (titration and potentiometry), total sulphate concentration (conductivity) and  $\text{NaClO}_4$  concentration (gravimetry). Experimental verifications were found to be in very good agreement with the data issued from the code.

Solvent extraction experiments were performed with protactinium (isotope  $^{233}\text{Pa}$  - 27d) at tracer scale (ca.  $10^{-12}\text{M}$ ) and TTA as chelating agent. The preparation of the organic (TTA/toluene) and the aqueous ( $\text{HClO}_4/\text{NaClO}_4/\text{Na}_2\text{SO}_4$ ) phases as well as the overall experimental protocol used in this work are identical to those used in the hydrolysis studies and are extensively described in References 3 to 5. The cumbersome experimental conditions developed in this work are necessary owing to the chemical properties of protactinium in non-complexing media. Although this protocol is time consuming, it allows reproducible results.

Extraction experiments were performed in the dark, in a temperature-controlled bath. Equal volumes of organic and aqueous phases (5 ml) and an aliquot of a freshly diluted solution of Pa(V) were introduced in glass containers, covered by a thin and homogeneous film of Galxyl-Parylene (COMELEC, Switzerland). After phase separation, the apparent distribution coefficient D was calculated as the ratio of the radioactivities in  $^{233}\text{Pa}$  in the organic towards the aqueous phases. For each D value, errors were derived.

The variations of the slope  $\partial(\log D)/\partial(\log C_{\text{H}^+})$  as a function of  $C_{\text{H}^+}$  for each value of  $C_{\text{TTA}}$  and  $C_{\text{SO}_4}$  give information about the mean charge of the predominant species in aqueous solution, while, the variation of  $\partial(\log D)/\partial(\log C_{\text{TTA}})$ , lead to the mean number of TTA molecules in the extracted complexes.

The sulphate complexation constants at fixed ionic strength, proton concentration and temperature, are deduced from the variations of D as a function of the free sulphate concentration, for a given value of TTA

concentration. Figure 1 depicts a typical set of experiments.

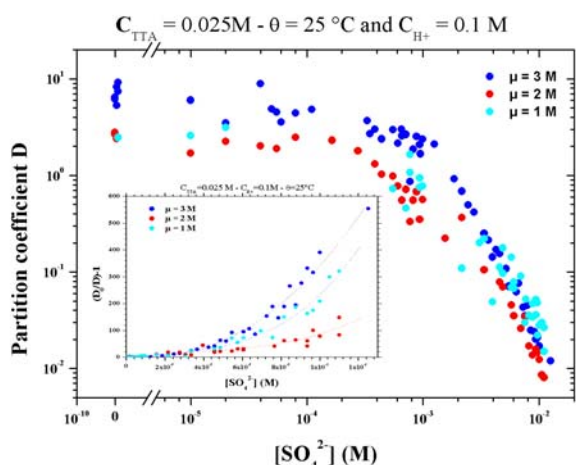


Fig. 1 : Variation of Pa(V) distribution coefficients, at tracer scale, as a function of free sulphate concentration.

Experiments are currently running and will lead to the determination of the complexation constant as a function of ionic strength, proton concentration and temperature. SIT modelling will be used in order to extract the complexation constants at infinite dilution and the SIT interaction coefficients  $\epsilon(i,j)$  of the sulphato-protactinium species (including temperature variations). Standard thermodynamical data ( $\Delta_r H^0$ ,  $\Delta_r C_p^0$ ,  $\Delta_r G^0$  and  $\Delta_r S^0$ ) will also be determined when sufficient data will be collected.

## 2 Structural measurements

This work is the first attempt to investigate the occurrence of the oxocation form of Pa(V) in  $H_2SO_4$  solutions. Protactinium measurements were carried out on the ROBL beam line at ESRF (6.0 GeV at 200 mA) in fluorescence mode, at room temperature and all data were acquired at the Pa  $L_{III}$  edge (16733 eV). Data fitting was carried out in R space without any prior data filtering with Artemis code. Phases and amplitudes were calculated by Feff8.2 code from crystallographic structures of  $Na_{10}[(UO_2)(SO_4)_4](SO_4)_2 \cdot 3H_2O$  (with  $Z=92$  replaced by  $Z=91$  in the Feff input file).

In the FT spectrum (fig 2), peak D is clearly attributed to a short Pa-ligand bond. Combining this result with the XANES data and simulation shows unambiguously that this sample exhibits a single short P-O bond in a monooxo form. Peak E contains second sphere O ligands and peak F originates from third sphere S ligands. Adjustment of the raw EXAFS spectrum was carried out according to the general formula  $PaO(SO_4)_n^{bid} (SO_4)_p^{mon}$  from  $n = 0$  to 3,  $p = 0$  to 7. Fits with only bidentate sulphates or only monodentate sulphates did not reproduce the experimental spectrum. Fits with  $n = 1$ ,  $p = 4$  or  $n = 3$ ,  $p = 1$  lead to a bad agreement and the optimum number for  $n$  was found to be 2.

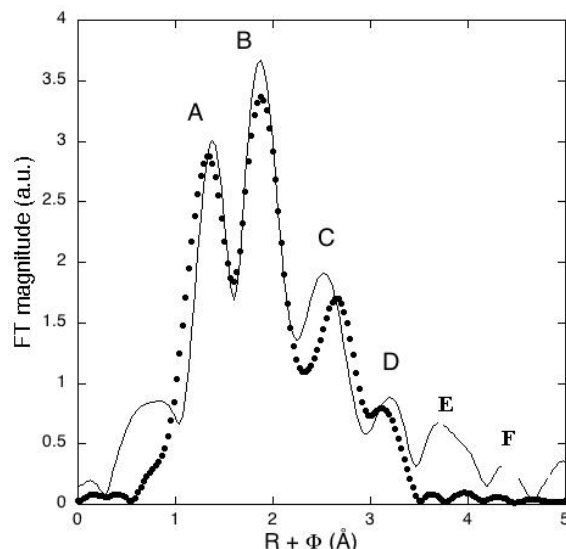


Fig. 2 : Fourier transform of  $L_{III}$  edge EXAFS spectra for Pa(V) in sulfuric solution (fitted curve  $\bullet\bullet\bullet\bullet\bullet\bullet$ ).

Within the uncertainty associated to amplitude estimation in EXAFS the fit is more sensitive to number  $n$  than to number  $p$  because  $n$  contributes for 2 oxygen atoms and one sulfur atom. The value of  $p$  has then been fixed to 3 but the uncertainty is about  $\pm 1$ . Best fit structural parameters were obtained with one Pa-O bond at 1.72 Å, two bidentate sulphate ligands at 2.41 Å and corresponding S atoms at 3.09 Å and 3 monodentate sulphate ligands at 2.33 Å and corresponding S atoms at 3.73 Å.

These results indicate unambiguously the presence of an oxo bound in  $H_2SO_4$  13 M medium as postulated for more dilute media where the species  $PaOSO_4^+$  and  $PaO(SO_4)_2^{2-}$  have been proposed [1,2]. Furthermore, the number of mono- and bi-dentate sulphate ligands deduced from EXAFS agrees with one of the formulations of the oxo-trisulphato-protactinate (V) proposed by Bagnall *et al.* [6]

- 1 R. Guillaumont, G. Boussières, and R. Muxart, *Actinides Rev.*, 1968, **1**, 135
- 2 R. Muxart, and R. Guillaumont, *Compléments au Nouveau Traité de Chimie Minérale-2-Protactinium*, Masson ed, Paris, 1974
- 3 D. Trubert, C. Le Naour, and C. Jaussaud, *J. Sol. Chem.* 2002, **31**, 261
- 4 C. Le Naour, D. Trubert, and C. Jaussaud, *J. Sol. Chem.* 2003, **32**, 489
- 5 C. Jaussaud, PhD thesis N° 7149, University Paris XI, France, 2003
- 6 Bagnall, K. W.; Brown, D.; Jones, P. J. *J. Chem. Soc.*, 1965, **27**, 176-181.

# Physicochemical properties of U(IV) chloro complexes in room temperature ionic liquids

**IPNO Participation:** C. Cannes, C. Le Naour, D. Trubert, S. Nikitenko

**Collaboration :** IPC Moscou, CEA Valrho et CEA Saclay, ESRF/ROBL Grenoble, Actinet Network

## Propriétés physicochimiques de complexes chlorés d'U(IV) dans les liquides ioniques à température ambiante

Les spectres d'absorption de  $[\text{BuMeIm}]_2[\text{UCl}_6]$  et  $[\text{MeBu}_3\text{N}]_2[\text{UCl}_6]$  respectivement dans  $[\text{BuMeIm}][\text{Tf}_2\text{N}]$  et  $[\text{MeBu}_3\text{N}][\text{Tf}_2\text{N}]$  sont similaires à ceux obtenus pour les solides par réflectance. Le complexe octaédrique  $\text{UCl}_6^{2-}$  serait donc la forme chimique prédominante dans les deux RTILs. Cette structure est confirmée par DRX et EXAFS et la distance de la liaison U-Cl est de 2.63 Å. L'analyse spectroscopique montre également la stabilité de ces complexes vis-à-vis de l'hydrolyse. Dans les deux liquides ioniques, les voltammogrammes de  $\text{UCl}_6^{2-}$  révèlent trois processus :  $\text{U}^{\text{V}}\text{Cl}_6^-/\text{U}^{\text{IV}}\text{Cl}_6^{2-}$ ,  $\text{U}^{\text{IV}}\text{Cl}_6^{2-}/\text{U}^{\text{III}}\text{Cl}_6^{3-}$  et  $\text{U}^{\text{IV}}\text{Cl}_6^{2-}/\text{U}^{\text{III}}\text{Cl}_6(\text{Tf}_2\text{N})_x^{-(3+x)}$ . Dans  $[\text{MeBu}_3\text{N}][\text{Tf}_2\text{N}]$ , un processus cathodique irréversible est aussi observé à -3.12 V/(Ag/Ag(I)) qui pourrait être attribué à la réduction de U(III) en U(0). De plus, la différence des potentiels rédox de U(V)/U(IV) et U(IV)/U(III) dans les deux liquides ioniques peut être expliquée par une solvation différente des complexes d'uranium :  $\text{BuMeIm}^+$  interagirait par liaison hydrogène de manière plus forte avec les complexes d'U(IV) que  $\text{MeBu}_3\text{N}^+$ .

Room Temperature Ionic Liquids (RTILs) are a new and remarkable class of solvents composed of organic cations and inorganic anions and their properties can be tailored by a suitable choice of cation/anion combination.<sup>1</sup> They display negligible vapour pressure, high thermal stability, high electrical conductivity and large electrochemical window. In principle, their use would allow actinide separation and purification processes capable of reducing the volume of radioactive waste and improving the safety of spent nuclear fuel reprocessing.<sup>2,4</sup> Most of the studies of actinide chemistry in RTILs have been performed in chloroaluminate based melts which are extremely sensitive to water and can be hardly used in radiochemistry. Recently, water stable RTILs with alkylimidazolium or tetraalkylammonium cations were synthesized.

We have then selected the 1-butyl-3-methylimidazolium ( $\text{BuMeIm}^+$ ) and the tri-n-butylmethylammonium ( $\text{MeBu}_3\text{N}^+$ ) cations associated with the inorganic anion  $(\text{CF}_3\text{SO}_2)_2\text{N}^-$  ( $\text{Tf}_2\text{N}^-$ ) to study the physicochemical properties of U(IV) hexachloro complexes in water stable RTILs. Two complexes are synthesized:  $[\text{BuMeIm}]_2[\text{UCl}_6]$  and  $[\text{MeBu}_3\text{N}]_2[\text{UCl}_6]$ . First, our work is focused on the determination by spectroscopy of the predominant chemical forms of U(IV) in both ionic liquids and their stability towards hydrolysis. Secondly, the uranium redox properties are studied and compared in the two ionic liquids to get information about the solvation of U(IV).

### 1 Structural investigation

The absorption spectra (Fig. 1) of  $[\text{BuMeIm}]_2[\text{UCl}_6]$  either in  $[\text{BuMeIm}][\text{Tf}_2\text{N}]$  and in acetonitrile, and  $[\text{MeBu}_3\text{N}]_2[\text{UCl}_6]$  in  $[\text{MeBu}_3\text{N}][\text{Tf}_2\text{N}]$  present the same absorption maxima. The diffuse solid state reflectance spectra of  $[\text{BuMeIm}]_2[\text{UCl}_6]$  and  $[\text{MeBu}_3\text{N}]_2[\text{UCl}_6]$

(Fig. 2) agree closely with the absorption spectra in solutions. It is well known that U(IV) hexachloro complex has a centrosymmetric octahedral arrangement in the solid state as well as in acetonitrile solution. Absorption bands have low intensities since electronic  $f \rightarrow f$  transitions are Laport forbidden. The octahedral anion  $\text{UCl}_6^{2-}$  would be the predominant form of U(IV) in  $\text{Tf}_2\text{N}^-$  based ionic liquids. This result is confirmed by EXAFS spectroscopy and X-ray diffraction. The U-Cl distance measured by EXAFS is 2.63 Å.

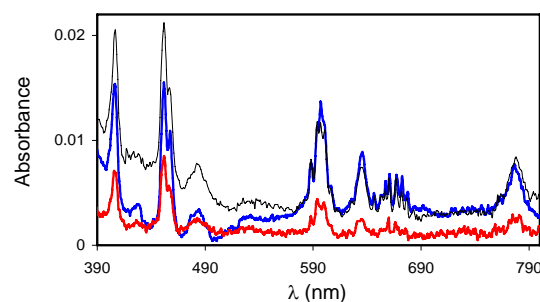


Fig. 1 : Absorption spectra of  $[\text{BuMeIm}]_2[\text{UCl}_6]$  (0.01 M) in  $[\text{BuMeIm}][\text{Tf}_2\text{N}]$ , in acetonitrile and  $[\text{MeBu}_3\text{N}]_2[\text{UCl}_6]$  (0.01 M) in  $[\text{MeBu}_3\text{N}][\text{Tf}_2\text{N}]$  at room temperature.

Moreover, the intensities of  $\text{UCl}_6^{2-}$  absorption bands are lower in acetonitrile than in RTILs. This can be attributed to stronger solvation of  $\text{UCl}_6^{2-}$  in ionic liquids compared with acetonitrile.

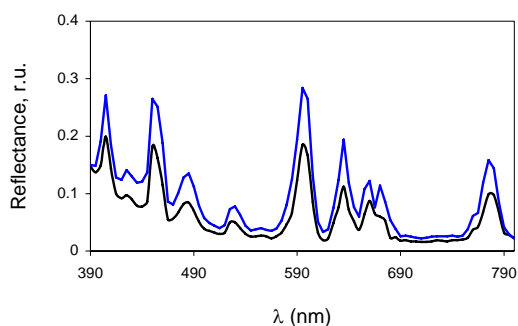
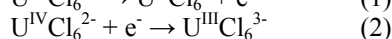
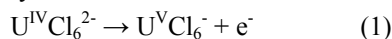


Fig. 2 : Diffuse solid state reflectance spectra of **[BuMeIm]<sub>2</sub>[UCl<sub>6</sub>]** and **[MeBu<sub>3</sub>N]<sub>2</sub>[UCl<sub>6</sub>]**.

In [BuMeIm][Tf<sub>2</sub>N], addition of water to 0.5M has no significant effect on the absorption spectrum of [BuMeIm]<sub>2</sub>[UCl<sub>6</sub>] indicating the stability of UCl<sub>6</sub><sup>2-</sup> with respect to hydrolysis in hydrophobic ionic liquids. This was explained by strong solvation of UCl<sub>6</sub><sup>2-</sup> anion in ionic liquids and by H-bonding of water molecules with Tf<sub>2</sub>N<sup>-</sup> anions.

## 2 Redox properties of U(IV) chloro complexes

Figure 3 shows that the electrochemical window of [BuMeIm][Tf<sub>2</sub>N] spans the potential range from -2.5 to 1 V vs. Ag/Ag(I). In this potential range, the voltammograms of UCl<sub>6</sub><sup>2-</sup> in [BuMeIm][Tf<sub>2</sub>N] at a glassy carbon working electrode reveals a system at 0.27 V and one at -1.96 V. Variation of the difference between the anodic and the cathodic peak with  $v$  as well as a linear dependence of the peak intensities on  $v^{1/2}$  ( $v$  : potential scan rate) indicate the quasi-reversibility of these systems. One can conclude that both U(IV) oxidation and reduction occurs without chloride ion transfer according to equation 1 and 2 respectively.



Moreover, the ratio between the anodic and the cathodic peak intensity for both systems shows the relative stability of the hexachloro complexes U<sup>V</sup>Cl<sub>6</sub><sup>-</sup> and U<sup>III</sup>Cl<sub>6</sub><sup>3-</sup>.

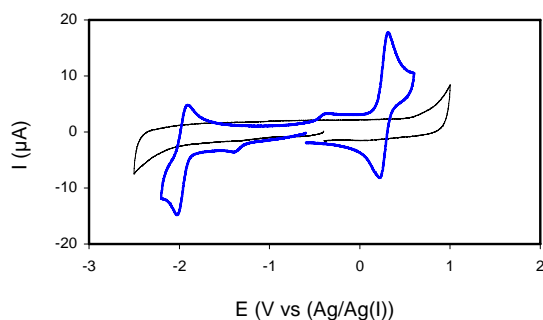
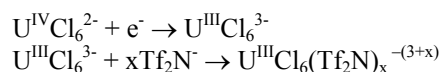


Fig. 3 : Cyclic voltammograms of **[BuMeIm][Tf<sub>2</sub>N]** alone and **in presence of 0.01 M [BuMeIm]<sub>2</sub>[UCl<sub>6</sub>]**.  $v = 0.1 \text{ V s}^{-1}$ ,  $T = 25^\circ\text{C}$ , GC electrode area  $0.07 \text{ cm}^2$ .

The voltammogram of U<sup>IV</sup>Cl<sub>6</sub><sup>2-</sup> in [BuMeIm][Tf<sub>2</sub>N] demonstrates also a reduction peak at -1.4 V and an oxidation peak at -0.4 V with a shoulder at -0.73 V. According to the electrochemical analysis, we have proposed the following mechanism:



Indeed, Tf<sub>2</sub>N<sup>-</sup> is known to be a weak ligand exhibiting oxygen coordination as η<sup>1</sup>-O or η<sup>2</sup>-O, O to actinides or lanthanides. The peak current for this process is lower than for the reduction at -1.96 V, indicating the relatively low yield of U(III) mixed-ligand species.

Fig. 4 shows that the electrochemical window of dried [MeBu<sub>3</sub>N][Tf<sub>2</sub>N] is still larger than that of [BuMeIm][Tf<sub>2</sub>N] and spans from -3.5 V to +1 V at a glassy carbon electrode. The cyclic voltammogram of [MeBu<sub>3</sub>N]<sub>2</sub>[UCl<sub>6</sub>] in [MeBu<sub>3</sub>N][Tf<sub>2</sub>N] (Fig. 4) reveals two redox systems with comparable intensities at +0.19 V and -2.2 V which can be attributed to the equation (1) and (2).

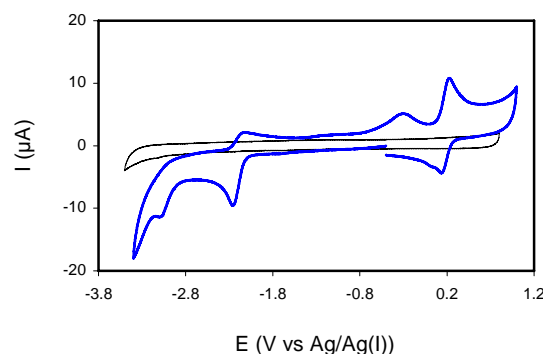


Fig. 4 : Cyclic voltammograms of **[MeBu<sub>3</sub>N][Tf<sub>2</sub>N]** alone and **in presence of 0.01 M [MeBu<sub>3</sub>N]<sub>2</sub>[UCl<sub>6</sub>]**.  $v = 0.1 \text{ V s}^{-1}$ ,  $T = 60^\circ\text{C}$ , GC electrode area  $0.07 \text{ cm}^2$ .

The electrochemical analysis in both ionic liquids shows that the uranium redox potential values depend strongly on the RTIL cation. Moreover, the U(IV)/U(III) redox couple is more sensitive to the RTIL cation than that of U(V)/U(IV) couple as the half-wave potential of the U(V)/U(IV) couple is 80 mV and those of U(IV)/U(III) 250 mV more positive in [BuMeIm][Tf<sub>2</sub>N] than in [MeBu<sub>3</sub>N][Tf<sub>2</sub>N]. This was attributed to the difference in solvation of uranium complexes in the two ionic liquids. These fundamental data indicate that the hydrophobic ionic liquids cannot be considered as inert solvents with respect to An(IV) hexachloro complexes.

Moreover, the cyclic voltammogram of UCl<sub>6</sub><sup>2-</sup> in [MeBu<sub>3</sub>N][Tf<sub>2</sub>N] exhibits a cathodic peak at -3.12 V vs. Ag/Ag(I) and an anodic peak at -0.16 V. The reduction wave could be attributed to the reduction of U(III) to U(0) and the anodic wave to the electrochemical redissolution of metallic uranium.

- 1 P. Wasserscheid, T. Welton, *Ionic Liquids in Synthesis*, Eds., Wiley : Weinheim, Germany, 2003.
- 2 A.E. Visser, R.D. Rogers, *J. of Solid State Chem.*, 2003, **109**, 113.
- 3 S. Dai, Y.H. Ju, C.E. Barnes, *J. Chem. Soc. Dalton Trans*, 1999, 1201.
- 4 M.L. Dietz, J.A. Dzielawa, *Chem. Commun.*, 2001, 2124

